Journal of Molecular Catalysis A: Chemical 320 (2010) 1–13

Contents lists available at ScienceDirect

Journal of Molecular Catalysis A: Chemical

journal homepage: www.elsevier.com/locate/molcata

Editor's choice paper

Properties of alkali-promoted Cu–MgO catalysts and their activity for methanol decomposition and C_2-oxygenate formation

Shahin Goodarznia, Kevin J. Smith*

Department of Chemical and Biological Engineering, The University of British Columbia, 2360, East Mall, Vancouver, BC, Canada V6T 1Z3

ARTICLE INFO

Article history:
Received 14 August 2009
Received in revised form
19 December 2009
Accepted 3 January 2010
Available online 13 January 2010

Keywords:
Catalyst
Promoter
Syngas
Cu–MgO
Basicity
Methyl formate
Ethanol
CO
Cu dispersion

ABSTRACT

The decomposition of CH_3OH in the presence of CO has been investigated over high surface area MgO, Cu–MgO, K–Cu–MgO and Cs–Cu–MgO catalysts. The catalysts were prepared by thermal decomposition of metal salts mixed with palmitic acid. The reduced catalysts had surface areas of 18–74 $m^2\,g^{-1}$ and intrinsic basicities of 4–17 $\mu mol\,CO_2\,m^{-2}$. Results revealed that methyl formate was a primary product of CH_3OH decomposition, whereas CO was a secondary product. Although selectivity to C_2 species (ethanol and acetic acid) was low (<5 C-atom %) at the low pressure (101 kPa) conditions of the present study, there was an optimum intrinsic basicity (9.5 $\mu mol\,CO_2\,m^{-2}$) at which the selectivity to C_2 species and methyl formate reached a maximum. The role of catalyst basic properties in the formation of C_2 species from CH_3OH is discussed.

1. Introduction

Current interest in the production and use of oxygenate fuels stems in part from a concern for the environmental impact of fossil fuels used in the transportation sector. A major concern in this regard, is the emission of NO_x and other toxic, ozone depleting chemicals from automobile exhausts. Attempts to reduce these emissions include the use of reformulated gasolines that in the past have contained small amounts of methyl tertiary butyl ether (MTBE). As MTBE is phased out and ethanol is seen as a potential alternative, there is an increased interest in new synthesis routes to ethanol. Although most of the world's ethanol is produced by fermentation, the process is expensive and energy inefficient due to intensive distillation steps [1,2]. An alternative approach, which also has significant potential to reduce greenhouse gas emissions associated with fossil fuels, is the selective conversion of biomass-derived syngas ($CO/CO_2/H_2$) to ethanol.

The low-temperature methanol synthesis from syngas, operated at 5–10 MPa and 473–573 K, is one of the most selective industrial processes carried out on a commodity scale [3–10]. During the last two decades, there has been significant research on the development of catalysts that shift the synthesis away from methanol and towards higher alcohols, especially C_2–C_4 alcohols [11–22]. Promotion of Cu–ZnO–Al_2O_3 low-temperature methanol synthesis catalysts with alkali metals, increases the higher alcohol yield and selectivity [14,20,22,23]. However, these catalysts produce mostly isobutanol with a low selectivity to ethanol. Mechanistic studies have shown that over these catalysts, the first C–C coupling step occurs over basic sites [14,24–28,31]. In addition, methyl formate has been identified as an important intermediate species for ethanol synthesis from syngas and methanol [14,27], the yield of which is enhanced by alkali promotion of Cu–ZnO [14]. It has also been shown that Cu plays an important role in methanol dehydrocoupling to methyl formate [29,30]. These mechanistic studies suggest that catalysts with higher basicity than alkali-promoted Cu–ZnO catalysts could potentially enhance the rate of the first C–C coupling step in alcohol synthesis and thereby increase selectivity to ethanol. Several studies have reported on the basicity of alkali promoted MgO [32–35], demonstrating that alkali promoted MgO possesses high basicity. For example, the basic site density of MgO has been reported as 2.2–7.2 $\mu mol\,CO_2\,m^{-2}$ [32–35] whereas for ZnO–ZrO_2 a value of 0.9 $\mu mol\,CO_2\,m^{-2}$ has been reported [36].

Noting the above properties of Cu, MgO, alkali promoters and the proposed mechanism of the first C–C bond formation step in alcohol synthesis from syngas, the present work has focused on alkali-promoted Cu–MgO catalysts to better understand the effect of

* Corresponding author. Tel.: +1 604 822 3601; fax: +1 604 822 6003.
E-mail address: kjs@interchange.ubc.ca (K.J. Smith).

1381-1169/$ – see front matter © 2010 Elsevier B.V. All rights reserved.
doi:10.1016/j.molcata.2010.01.002

increased basicity on the mechanistic pathways to C_2 species from C_1 species (CH_3OH and CO). In the first part of the study, the preparation and characterization of high surface area, alkali-promoted Cu–MgO catalysts is reported. Subsequently, the activity of these catalysts for methanol decomposition and C–C bond formation has been determined. The synthesis of alcohols from syngas is usually done at high pressures (>5 MPa) to overcome thermodynamic yield limitations of the methanol synthesis [14,20,22,23]. In the present work, however, low pressure (101 kPa) has been used to simplify the experimental procedures. Furthermore, by using CH_3OH as reactant and operating at low pressure, the decomposition of the feed CH_3OH that will generate surface species that can react further to produce C_2 species, is assured. A related study of ethanol and higher alcohol formation from CH_3OH over a Cu–MgO–Al_2O_3 catalyst, reported recently, also used low pressure (101 kPa) [37]. Although no catalytic activity towards ethanol and higher alcohols was reported, dimethyl ether was produced.

In the present work, we report on the products generated from reactions of CH_3OH in the presence of CO, H_2 or He, at low pressure (101 kPa) as a function of the alkali-promoted Cu–MgO catalyst properties and use these data to provide insights into potential pathways for higher ethanol selectivity in syngas conversion. In future work, the same catalysts will be examined under high pressure conditions for syngas conversion.

2. Experimental

2.1. Catalyst preparation

High surface area, MgO, Cu–MgO, alkali-promoted Cu–MgO (0.5 wt% K–Cu–MgO, 4.4 wt% K–Cu–MgO, 0.5 wt% Cs–Cu–MgO and 13.5 wt% Cs–Cu–MgO) and bulk CuO were prepared by thermal decomposition of metal salts in the presence of palmitic acid ($CH_3(CH_2)_{14}COOH$) [38]. Note that the 4.4 wt% K and the 13.5 wt% Cs promoted Cu–MgO catalysts had the same alkali/Mg molar ratio of 0.08. $Mg(NO_3)_2{\cdot}6H_2O$, $Cu(NO_3)_2{\cdot}3H_2O$, Cs_2CO_3 and KNO_3 were used as the source of MgO, Cu, Cs_2O and K_2O, respectively. The molar ratio of palmitic acid to [Mg + Cu + alkali metal] was 2.5 [38]. Note that in all cases the catalysts were nominally 40 wt% Cu and 60 wt% MgO when in the reduced state. As an example, to prepare the 0.5 wt% Cs–Cu–MgO catalyst, 6.00 g of $Mg(NO_3)_2{\cdot}6H_2O$ (Sigma–Aldrich, 99%), 2.47 g of $Cu(NO_3)_2{\cdot}3H_2O$ (AlfaAesar, 98–102%), 0.01 g Cs_2CO_3 (Sigma–Aldrich, 99%) and 21.89 g palmitic acid (Sigma–Aldrich, 98%) were mechanically mixed in a crucible without adding water and placed in a furnace (Barnstead/Thermolyne 47900) in air at ambient pressure. The mixture was heated to 373 K for 60 min at 40 K min^{-1} followed by heating to 445 K for 60 min at 40 K min^{-1}. The solid catalyst precursor was obtained by subsequent calcination at 673 K. Calcination was achieved at a heat up rate of 0.8 K min^{-1} and the final temperature was held for 300 min before cooling to room temperature. Finally, the catalyst precursor was reduced by heating to 573 K at a rate of 10 K min^{-1} in 10% H_2/He, with the final temperature held for 60 min in 100% H_2, yielding 1.59 g of the 0.5 wt% Cs–Cu–MgO catalyst.

Note that the final calcination temperature used for each catalyst precursor was determined by the highest decomposition temperature of the metal nitrates or carbonates present in the precursor. For MgO, Cu–MgO, K–Cu–MgO and Cs–Cu–MgO the calcination temperatures were 673 K, 673 K, 873 K and 923 K, respectively. The effect of calcination temperature, calcination time and the amount of palmitic acid used in the preparation of the MgO was also examined. In addition, one sample of MgO was prepared without the use of palmitic acid and consequently, in this case, the thermal treatment prior to calcination that was conducted on the MgO-based catalysts (373 K for 60 min and 445 K for 60 min) was not necessary.

2.2. Catalyst characterization

Temperature-programmed reduction (TPR) of the prepared catalyst precursors was performed in a 10% H_2/Ar gas flow of 50 cm^3(STP) min^{-1} and heating at a ramp rate of 10 K min^{-1} from 313 K to 623 K, with the final temperature held for 30 min. Prior to the TPR, samples (about 0.2 g) were pre-treated thermally in He at 50 cm^3(STP) min^{-1} and 393 K. Hydrogen consumption was monitored by a thermal conductivity detector (TCD) attached to a Micromeritics AutoChem II chemisorption analyzer. During the analysis the effluent gas was passed through a cold trap placed before the TCD in order to remove water from the exit stream of the reactor. Both CuO and Cu_2O (97% purity, particle size < 5 μm, Sigma–Aldrich) were also examined by TPR.

Catalyst BET surface areas were measured before and after reduction whereas the catalyst pore volume and pore diameter were measured before reduction only. The mentioned properties of the un-reduced catalysts were determined from N_2 adsorption–desorption isotherms measured at 77 K using a Micromeritics ASAP 2020 analyzer. Catalysts were degassed in 523 K for 24 h under vacuum (5 μm Hg) before being analyzed. Eight N_2 uptake measurements made in the range $0.06 < P_{N_2}/P^0_{N_2} < 0.20$ were used to calculate the BET surface area. The uptake of N_2 at $P_{N_2}/P^0_{N_2} = 0.975$ was used to specify the catalyst pore volume. Pore diameter was calculated based on the pore size distribution measured from the N_2 desorption in the range of $0.01 < P_{N_2}/P^0_{N_2} < 0.99$.

The BET surface area of the reduced catalysts was measured using the Micromeritics AutoChem II chemisorption analyzer. The catalysts were first degassed in 50 cm^3(STP) min^{-1} He by heating from ambient temperature to 523 K and holding at 523 K for 120 min. The catalysts were then cooled to room temperature and the feed gas was switched from He to 10% H_2 in Ar at a flow rate of 50 cm^3(STP) min^{-1}. The TPR analysis described above was then conducted on the catalyst. Since MgO adsorbs CO_2 and H_2O, pretreatment in He at high temperature (773 K) was required [39–41] after reduction and prior to the surface area measurement. Hence the gas flow was switched from 10% H_2 in Ar to He at a flow rate of 50 cm^3(STP) min^{-1} and heated to 773 K at a rate of 10 K min^{-1} for 60 min. The catalysts were then cooled to room temperature and the feed gas switched from He to 30 vol% N_2 in He at a flow rate of 50 cm^3(STP) min^{-1}. The single point BET surface area of the reduced catalyst was calculated by measuring the N_2 uptake of the catalyst at 77 K using the liquid N_2 trap.

Basic properties of the reduced catalysts were determined by CO_2 temperature-programmed desorption (TPD) using a Micromeritics AutoChem II chemisorption analyzer. The reduced catalysts were pre-treated thermally by ramping to 773 K at 10 K min^{-1} for 60 min in 50 cm^3(STP) min^{-1} of He. After cooling to 313 K, the sample was exposed to 50 cm^3(STP) min^{-1} of 10 vol% CO_2/He for 60 min. Physically adsorbed CO_2 was subsequently removed from the sample by flushing in He (50 cm^3(STP) min^{-1}) at 313 K for 60 min. The catalyst's basic properties were evaluated by observing the capacity of the samples to retain the CO_2 during the desorption that occurred in the He flow while increasing temperature from 313 K to 803 K at a rate of 10 K min^{-1}. The obtained CO_2 TPD profile was integrated to determine the catalyst intrinsic basicity, defined as the total CO_2 uptake divided by the BET surface area, and taken as a measure of the catalyst basic site density. To quantify the strength of the basic sites, the CO_2 TPD profiles were de-convoluted to classify weak (353–373 K), medium (373–473 K) and strong (>473 K) basic sites according to their temperature of desorption.

X-ray powder diffraction (XRD) patterns of the prepared catalysts were obtained with a Rigaku Multiflex diffractometer using Cu Kα radiation (λ = 0.154 nm, 40 kV and 20 mA), a scan range of 2θ

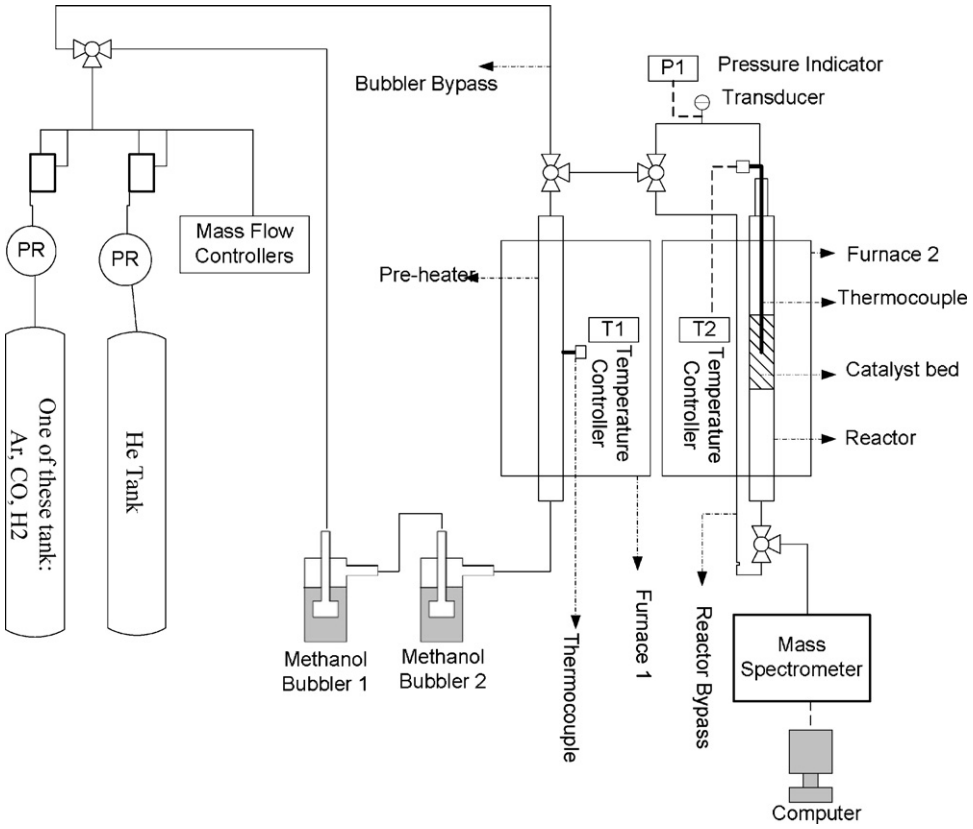

Fig. 1. Schematic diagram of the reactor setup.

from 10° to 100° and a step size of 2° per min. Crystallite size of the metal or metal oxide was estimated from the XRD data using the Scherrer equation. The Cu crystallite thickness (d_{Cu}^{XRD}) was estimated from the CuO crystallite size (d_{CuO}^{XRD}) determined from the XRD data of the non-reduced MgO-based catalysts, and the peak broadening at $2\theta = 35.5°$. The Cu crystallite size was then estimated as: $d_{Cu}^{XRD} = (\text{Cu molar volume/CuO molar volume}) \times d_{CuO}^{XRD}$. The MgO crystallite size (d_{MgO}^{XRD}) was measured based on the peak broadening at $2\theta = 42.9°$.

The Cu dispersion of the reduced catalysts was measured by adsorption and decomposition of N_2O on the surface of Cu according to the stoichiometry: $2Cu^0 + N_2O \rightarrow N_2 + Cu_2O$. The pulse titration technique was used. Following reduction, the catalysts were pre-treated thermally by heating to 773 K at a rate of 10 K min^{-1} for 60 min in a flow of 50 cm^3(STP) min^{-1} of He. The catalysts were then cooled to room temperature before the N_2O pulse titration was initiated using 10% N_2O/N_2 as the pulse gas. A TCD attached to a Micromeritics AutoChem II chemisorption analyzer was used to detect the consumption of N_2O and Cu dispersion was calculated from the total amount of N_2O consumed. A liquid Ar trap was used to condense N_2O from N_2 in the effluent, and hence only the N_2 was detected by the TCD.

2.3. Catalyst testing

Catalyst testing was conducted in a stainless steel fixed bed tubular reactor shown in Fig. 1, operated at atmospheric pressure with inert He and Ar mixed with CO, H_2 and CH_3OH as reactants. The catalyst (0.1–1.98 g) was loaded into the isothermal section of the reactor and reduced in 10% H_2/He at a flow rate of 100 cm^3(STP) min^{-1} and a ramp rate of 10 K min^{-1} from ambient temperature to 573 K. After further heating in pure He to 773 K, the reactor was cooled to the desired reaction temperature. The desired reactant gases at a total flowrate of 72 cm^3(STP) min^{-1} passed through two saturators in series containing pure CH_3OH at ambient temperature to generate the CH_3OH vapor (12 cm^3(STP) min^{-1}). The feed mixture then passed through a pre-heater at 383 K before entering the reactor. The gas flow lines between the pre-heater and the reactor as well between the reactor and the mass spectrometer were held at the same temperature as the pre-heater (383 K) using heating tapes. The reactor product composition was determined using a VG ProLab quadrupole mass spectrometer that continuously monitored the reactor exit gas line. In the present work, the focus was on the initial activity of the catalysts that were to be related to the properties of the fresh catalysts. Hence, after a 10 min reactor

Table 1
Effect of calcination temperature, calcination time and palmitic acid content on BET surface area, pore volume and pore size of MgO.

Catalyst	Calcination temperature (K)	Calcination time (min)	R[a] (–)	S_{BET}[b] (m^2 g^{-1})	V_p[b] (cm^3 g^{-1})	d_p[b] (nm)
MgO[c]	673	300	2.5	160	0.58	14.5
MgO-1	723	300	2.5	132	0.46	14.2
MgO-2	673	480	2.5	150	0.52	13.9
MgO-3	673	480	1.25	160	0.41	10.3
MgO-4	673	480	0.00	7	0.02	8.9

[a] R is molar ratio of palmitic acid to Mg + Cu + alkali metal.
[b] S_{BET}, V_p and d_p are respectively, BET surface area, pore volume and average pore size of MgO catalyst before reduction.
[c] These conditions have been used for preparation of all Cu–MgO-based catalysts of the present study.

Table 2
BET surface area, pore volume and pore size of alkali-promoted Cu–MgO catalysts.

Catalyst	Catalyst composition (A/Cu/MgO)[a] (wt%)	S_{BET}[b] ($m^2\ g^{-1}$)		V_p[b] ($cm^3\ g^{-1}$)	d_p[b] (nm)
		Before reduction	After reduction		
Cu–MgO	0/40.3/59.7	62	74	0.23	15.0
0.5 wt% K–Cu–MgO	0.5/40.1/59.3	35	42	0.20	23.1
0.5 wt% Cs–Cu–MgO	0.5/40.1/59.4	38	44	0.20	20.8
4.4 wt% K–Cu–MgO	4.4/38.2/56.5	26	30	0.17	26.4
13.5 wt% Cs–Cu–MgO	13.5/34.6/51.1	15	18	0.06	16.1

[a] *A* is alkali metal.
[b] S_{BET}, V_p and d_p are respectively, BET surface area, pore volume and average pore size of MgO catalyst before reduction.

stabilization period, data were collected over the next 10 min and the average of these analyses are reported herein. Both diagnostic tests and calculation were used to confirm that at the chosen conditions, the catalyst activity data were free of both internal and external heat and mass transfer effects. For each experiment the performance of the catalyst was compared to an identical experiment conducted in the absence of the catalyst so that the effect of thermal reactions or activity from the wall of the reactor were accounted for. The data reported herein are net of the blank run conversions and product yields. In each experiment conversion was defined as the total C-atom conversion of CH_3OH or [$CH_3OH + CO$] in the case that CO was present in the feed. In most cases however, there was no net CO consumption since CH_3OH decomposed mostly to CO. The product yield was calculated as the product of the total exit molar flow rate and the component mole fraction. Component selectivity was determined as the total C-atom conversion divided by the product yield.

3. Results and discussion

3.1. Catalyst characterization

The effect of preparation conditions on the properties of the MgO are reported in Table 1. Increased calcination temperature or calcination time decreased the BET surface area (S_{BET}) and the pore volume (V_p) of the MgO, most likely due to thermal sintering of the MgO crystallites. The S_{BET} results of Table 1 also show that a decrease in the mole fraction of palmitic acid used in the catalyst preparation led to an increase in the S_{BET} of the MgO. Following calcination, the MgO was grey in color, indicative of some carbonaceous residue from the palmitic acid not completely removed during calcination. With less palmitic acid, a lighter grey powder was produced, indicative of less carbonaceous impurity. The carbonaceous residue was likely responsible for the small decrease in surface area (through pore blockage) as the amount of palmitic acid increased. Note that the color of the MgO obtained from the thermal decomposition of $Mg(NO_3)_2{\cdot}6H_2O$ in the absence of palmitic acid was white (Table 1, MgO-4). Cosimo et al. [34] prepared MgO by thermal decomposition of $Mg(OH)_2$ in a high flow of air and reported an MgO surface area of 119 $m^2\ g^{-1}$, whereas the S_{BET} of MgO of the present study was 160 $m^2\ g^{-1}$ (Table 1, MgO) and the thermal decomposition of $Mg(NO_3)_2{\cdot}6H_2O$ in the absence of palmitic acid (Table 1, MgO-4) yielded MgO with a S_{BET} of 7 $m^2\ g^{-1}$. These results show the advantage of using palmitic acid to obtain higher surface area MgO. Palmitic acid plays an important role by limiting the sintering of the MgO, likely due to the fact that palmitic acid is a good chelating agent for Mg^{2+}. The method used herein to obtain high surface area MgO is more convenient and simpler than conventional thermal decomposition methods, wherein high flows of purge gas are typically required to remove produced water and thereby limit sintering of the MgO [34].

The properties of the alkali-promoted Cu–MgO catalysts are reported in Table 2. Compared to the data of Table 1 for MgO, the data show that addition of Cu to the MgO resulted in a loss of more than 50% of the MgO S_{BET} and V_p. The loss in S_{BET} and V_p could be partially due the fact that the CuO blocks the pores of the MgO, as suggested by others [42]. The pore size distributions of the MgO-based catalysts after calcination are shown in Fig. 2. The addition of the Cu to the MgO led to a significant increase in pore size, with the maxima of the pore size distribution occurring at much higher pore size compared to MgO (Fig. 2a, b). This supports the assertion that the smaller pores of the MgO were blocked by the CuO (before reduction). Nonetheless, the preparation method used herein yielded Cu–MgO with relatively high surface areas. For example, Nagaraja et al. [44] used co-precipitation to prepare Cu–MgO (nominally 40 wt% Cu and 60 wt% MgO) and reported an S_{BET} of 28 $m^2\ g^{-1}$ [44], whereas in the present study the S_{BET} of the Cu–MgO was 62 $m^2\ g^{-1}$ and 74 $m^2\ g^{-1}$ before and after reduction, respectively. For all of the prepared catalysts of Table 2, the S_{BET} increased by about 20% after reduction, a result of the water loss associated with the reduction of CuO to Cu. The catalyst average pore size (d_p) of the Cu–MgO catalysts, also reported in Table 2, shows that all of the prepared catalysts were mesoporous.

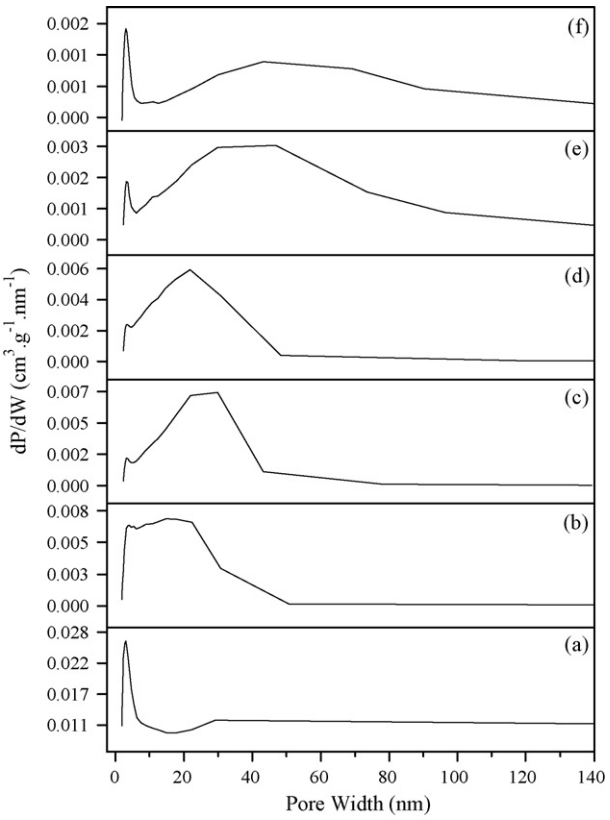

Fig. 2. Pore size distribution of un-reduced Cu–MgO-based catalysts: (a) MgO; (b) Cu–MgO; (c) 0.5 wt% K–Cu–MgO; (d) 0.5 wt% Cs–Cu–MgO; (e) 4.4 wt% K–Cu–MgO; (f) 13.5 wt% Cs–Cu–MgO.

Addition of Cs or K to the Cu–MgO also decreased the S_{BET} and V_p. Noting that the K promoted Cu–MgO and the Cs promoted Cu–MgO precursors were calcined at higher temperatures than the MgO and the Cu–MgO, it is likely that thermal sintering contributed to the decreased S_{BET} and V_p of the alkali-promoted Cu–MgO. Table 2 also shows that increasing the K loading of the K–Cu–MgO catalyst from 0.5 wt% to 4.4 wt%, decreased the catalyst S_{BET} and V_p. Similar effects were observed for the Cs promoted Cu–MgO catalyst as the Cs loading increased from 0.5 wt% to 13.5 wt%. Pore blockage of MgO by Cs_2O or K_2O has been reported in the literature [42] and the trends observed with increased promoter concentration suggest that similar effects are important here as well. The pore size distribution data of Fig. 2c, e show that increasing the K loading of the K promoted Cu–MgO catalyst from 0.5 wt% to 4.4 wt%, led to a significant increase in pore size with the maxima of the pore size distribution occurring at a higher pore size with increased K. The same trend was observed as the Cs loading of the Cs–Cu–MgO was increased from 0.5 wt% to 13.5 wt% (Fig. 2c, e). These observations support the assertion that the decreased S_{BET} of the K or Cs promoted Cu–MgO, compared to the Cu–MgO, was partially due to MgO pore blockage by K_2O or Cs_2O. Also, note that the melting point and boiling point of palmitic acid are 336 K and 623 K, respectively [43] whereas for $Cu(NO_3)_2{\cdot}3H_2O$ the melting point and boiling point are 387 K and 443 K, respectively [43]. Clearly both the $Cu(NO_3)_2{\cdot}3H_2O$ and the palmitic acid are mixed in the liquid phase below 443 K, the temperature to which the catalyst precursors were heated during preparation. KNO_3 has a melting point and boiling point of 607 K and 673 K, respectively [43] whereas Cs_2CO_3 is reported to decompose in the temperature range of 823–873 K to Cs_2O [45]. Hence, although the alkali promoters may be below their melting points during the mixing of the components at elevated temperatures, the promoters are likely solubilized by the palmitic acid during synthesis of the promoted Cu–MgO catalysts, and this ensured that the promoters were well dispersed throughout the catalysts.

Fig. 3 shows the X-ray diffractograms of the MgO-based catalyst precursors, measured after calcination but prior to reduction. The data confirmed the presence of MgO (periclase, Fm3m(225)-cubic structure) and CuO (tenorite, C2/c(15) monoclinic structure) and the absence of Cu_2O in the precursor samples. In addition, no peaks associated with alkali metal oxides were observed, either because the alkali promoter was below the XRD detection limit (for the 0.5 wt% K and Cs samples) or they were present as amorphous, well dispersed alkali metal oxides (for the 4.4 wt% K and 13.5 wt% Cs samples). Using the data of Fig. 3, the MgO crystallite thickness (d^{XRD}_{MgO}) and Cu crystallite thickness (d^{XRD}_{Cu}) were estimated and the results are shown in Table 3. Both d^{XRD}_{MgO} and d^{XRD}_{Cu} increased in the same order that the S_{BET} of the MgO-based catalysts decreased, indicating that the loss in S_{BET} was also partly due to thermal sintering of the MgO and the Cu.

The unit cell size of the MgO (a_{MgO}) was calculated from the XRD data for all of the MgO-based catalysts using the formula: $a_{MgO} = 2d^{XRD}_{MgO}$ since MgO has a cubic crystal structure. As shown in Table 3, the same unit cell size was obtained for all of the catalysts, indicating that there was no solid solution present in the un-reduced Cu–MgO-based catalyst precursors. Hence it can be concluded that MgO and CuO crystallites were present as separate phases in the prepared catalysts.

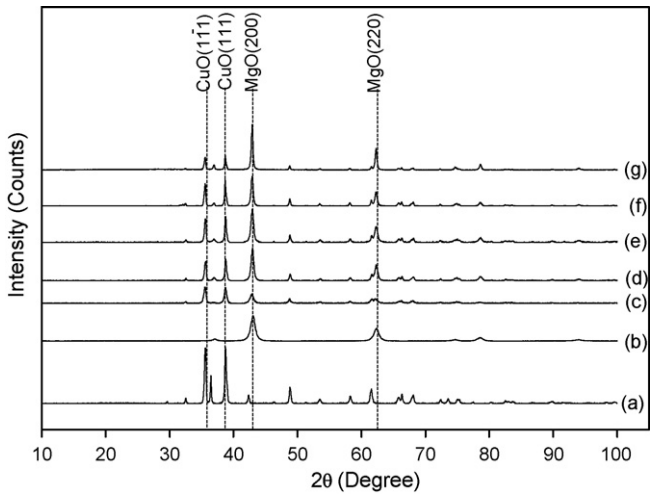

Fig. 3. X-ray diffractograms of un-reduced MgO-based catalysts: (a) CuO; (b) MgO; (c) Cu–MgO; (d) 0.5 wt% K–Cu–MgO; (e) 0.5 wt% Cs–Cu–MgO; (f) 4.4 wt% K–Cu–MgO; (g) 13.5 wt% Cs–Cu–MgO.

The Cu dispersion of the Cu–MgO-based catalysts, reported in Table 3, show that for all of the catalysts the Cu dispersion was low (<2%). The Cu–MgO had the highest Cu dispersion among all of the prepared catalysts and addition of K_2O or Cs_2O decreased Cu dispersion. The Cu crystallite size ($d^{N_2O}_{Cu}$) as inferred from the N_2O adsorption–decomposition analysis was significantly higher than that determined from the XRD analysis (d^{XRD}_{Cu}), implying that most of the Cu crystallites (diameter < 30 nm), were occluded from the catalyst surface and not active to N_2O titration. The high Cu loading (>34.6 wt%) in the prepared Cu–MgO-based catalysts is the likely cause, resulting in significant agglomeration of CuO crystallites. Cu thermal sintering at the higher calcination temperatures used for the alkali-promoted Cu–MgO catalysts, compared to the unpromoted Cu–MgO catalyst, also contributed to the lower Cu dipersion of the alkali-promoted Cu–MgO compared to the unpromoted Cu–MgO.

The TPR profiles of the calcined catalyst precursors of the present study are reported in Fig. 4 and the reduction peak temperatures and calculated degrees of reduction are summarized in Table 4. For comparison, the TPR profiles of CuO and Cu_2O are also reported in Fig. 4 and Table 4. The CuO TPR profiles showed that bulk CuO had a reduction peak maximum at 516 K, in agreement with the literature [46]. The Cu_2O TPR profile showed a reduction peak maximum at 594 K. The degree of reduction for Cu_2O was 100% whereas the degree of reduction for CuO was 88%. The nominal particle size of all of the laboratory prepared catalysts as well as the bulk CuO of the present study was 267 μm, whereas the Cu_2O particle size was 5 μm. Hence it is likely that complete reduction of the CuO was hindered by H_2 diffusion to the core of the larger, partially reduced Cu–CuO particle. Assuming CuO as the only reducible species present in the calcined catalyst precursors,

Table 3
Copper dispersion, crystallite size and MgO unit cell size of catalysts as determined by N_2O pulse titration and XRD.

Catalyst	Cu dispersion (%)	$S^{N_2O}_{Cu}$ ($m^2\ g^{-1}$)[a]	$d^{N_2O}_{Cu}$ (nm)	d^{XRD}_{Cu} (nm)	d^{XRD}_{MgO} (nm)	a_{MgO} (nm)
MgO	–	–	–	–	13	0.42
Cu–MgO	1.54	2.64	65	15	17	0.42
0.5 wt% K–Cu–MgO	0.19	0.50	519	21	20	0.42
0.5 wt% Cs–Cu–MgO	0.28	0.58	362	24	20	0.42
4.4 wt% K–Cu–MgO	0.24	0.60	420	26	24	0.42
13.5 wt% Cs–Cu–MgO	0.52	0.76	194	27	32	0.42

[a] Copper metal surface area was calculated assuming 1.46×10^{19} copper atoms per m^2.

Table 4
Temperature-programmed reduction results for Cu–MgO-based catalysts.

Sample	Hydrogen consumption (mmol g^{-1} catalyst)	Distribution of different copper oxide species[a] (%)		Degree of reduction (%)	Reduction peak temperature (K)	
		1	2		T_1	T_2
Cu_2O	6.84	100	–	100	594	–
CuO	11.06	100	–	88	516	–
Cu–MgO	5.08	87	13	88	512	535
0.5 wt% K–Cu–MgO	4.77	69	31	83	506	539
0.5 wt% Cs–Cu–MgO	4.89	73	27	85	518	552
4.4 wt% K–Cu–MgO	4.56	71	29	83	512	535
13.5 wt% Cs–Cu–MgO	4.20	90	10	84	538	578

[a] Copper oxide species corresponded to CuO in all cases except for Cu_2O catalyst.

the TPR results of the Cu–MgO-based catalysts revealed that, in all cases, the degree of reduction was more than 80%. However, due to an interaction between the alkali metal oxide, the MgO and the CuO, 100% reduction of the CuO was not achieved and two different reduction temperatures were observed. The TPR profiles were therefore de-convoluted (Fig. 4) to quantify each of the CuO species. Except for the 13.5 wt% Cs–Cu–MgO, the first reduction peak occurred in the range of 506–518 K and the second reduction peak occurred in the range of 535–552 K. The first reduction peak was attributed to bulk CuO reduction and the second was assigned to CuO species that interacted with MgO and/or the alkali promoters and were consequently, more difficult to reduce. The weak CuO interaction with bulk MgO and its inhibiting effect on Cu reduction has been reported previously [46–48]. Addition of the alkali promoters to Cu–MgO led to more CuO species that were more difficult to reduce, indicative of the K_2O and Cs_2O interaction with the CuO. The phenomenon of alkali metal oxide interaction with CuO and its inhibiting effect on CuO reduction, has also been noted in previous studies [49] and is apparent for all the alkali-promoted Cu–MgO catalysts reported in Table 4. The TPR profile of the 0.5 wt% K–Cu–MgO showed reduction peaks at 506 K and 539 K with a significant increase in the CuO species reduced at high temperature compared to the case of Cu–MgO. The TPR profile of the 0.5 wt% Cs–Cu–MgO showed reduction peaks at 518 K and 552 K and although these temperatures were slightly higher than for the 0.5 wt% K–Cu–MgO, the relative amounts of the two types of CuO species were very similar. Comparison of the TPR profile for 0.5 wt% K–Cu–MgO and 4.4 wt% K–Cu–MgO showed almost identical results, suggesting that increased K loading did not influence the interaction of K_2O with the CuO. However, the TPR profile of the 13.5 wt% Cs–Cu–MgO showed reduction peaks at 538 K and 578 K, significantly higher than for the other catalysts of Table 4. The first reduction peak was most likely due to the Cs_2O interaction with CuO described earlier. It is noticeable that except for the case of 13.5 wt% Cs–Cu–MgO, all of the Cu–MgO-based catalysts showed reduction peaks below the Cu_2O reduction peak temperature. This suggests that the high loading of Cs (13.5 wt%) led to the formation of a small amount of Cu_2O (<10 wt%) in the Cs–Cu–MgO catalyst that was not detectible by XRD, but that led to the second reduction peak in the TPR profile that corresponded to the reduction peak for bulk Cu_2O. The non-Gaussian TPR profile of the Cu–MgO-based catalysts (Fig. 4) has been attributed to different Cu oxide species present in the catalyst that reduce at different temperatures (Table 4). However, the presence of a heterogeneous size distribution of copper particles in the Cu–MgO catalyst may also contribute to the shape of the TPR curves, although in this case, higher N_2O uptakes from the smallest reduced Cu species would be expected to yield much higher overall N_2O uptakes than that reported in Table 3.

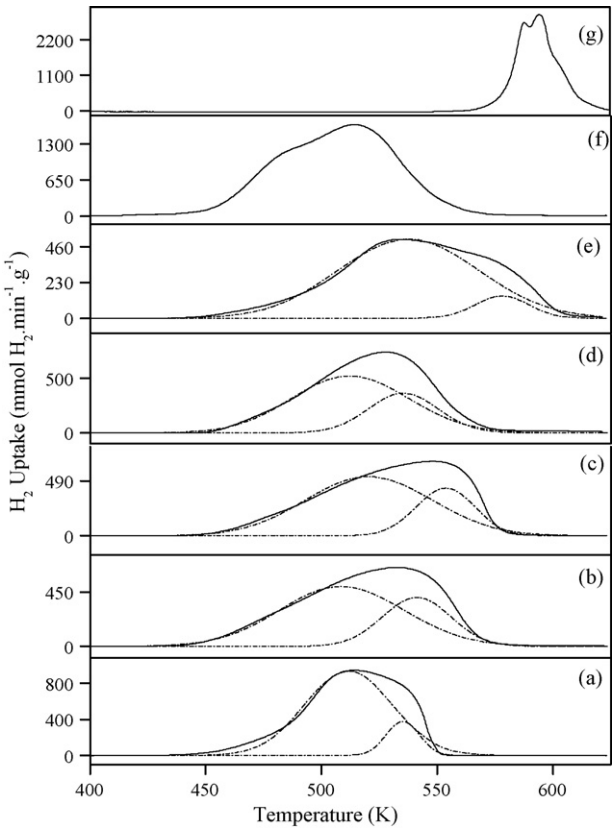

Fig. 4. Temperature program reduction profile for: (a) 40.1Cu–MgO; (b) 0.5 wt% K–Cu–MgO; (c) 0.5 wt% Cs–Cu–MgO; (d) 4.4 wt% K–Cu–MgO; (e) 13.5 wt% Cs–Cu–MgO; (f) CuO; (g) Cu_2O.

The CO_2 TPD profiles for all of the catalysts, shown in Fig. 5, were used to determine the catalyst intrinsic basicity and distribution of basic sites, as summarized in Table 5. The intrinsic basicity increased in the order: MgO < Cu–MgO < 0.5 wt% K–Cu–MgO < 0.5 wt% Cs–Cu–MgO < 4.4 wt% K–Cu–MgO < 13.5 wt% Cs–Cu–MgO and follows the expected trend, based on the known basicities of K, Cs and MgO. MgO had an intrinsic basicity of 2.7 μmol CO_2 m^{-2} in agreement with the MgO basicity reported in the literature [32–35]. Addition of Cu to the MgO increased the intrinsic basicity but the distribution of basic sites was almost unchanged. Addition of alkali metal (0.5 wt% Cs or K) to the Cu–MgO catalyst more than doubled the intrinsic basicity but the distribution of basic sites remained almost unchanged. The 4.39 wt% K–Cu–MgO catalyst had higher intrinsic basicity compared to the 0.50 wt% K–Cu–MgO catalyst, as well as a slightly higher percentage of weak basic sites, and similar trends were observed for the Cs–Cu–MgO catalyst. Therefore it can be concluded that in all cases, addition of alkali promoter to the Cu–MgO catalyst increased the intrinsic basicity but the effect on the distribution of basic sites was much less significant.

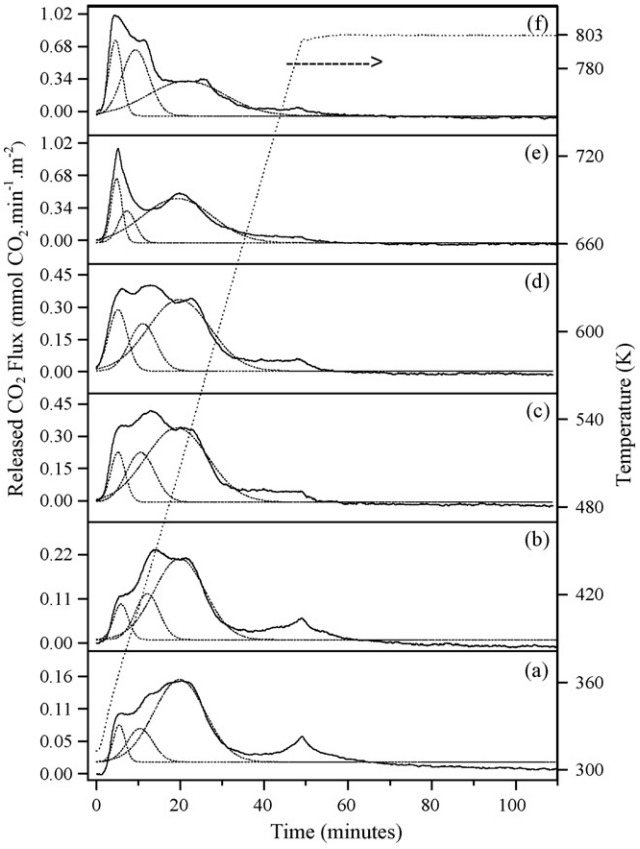

Fig. 5. CO_2 temperature program desorption of (a) MgO;(b) Cu–MgO; (c) 0.5 wt% K–Cu–MgO; (d) 0.5wCs–40.1Cu–MgO; (e) 4.4 wt% K–Cu–MgO; (f) 13.5 wt% Cs–Cu–MgO.

The basicity of an oxide surface is generally related to the electron donating properties of the combined oxygen anions, so that the higher the partial negative charge on the combined oxygen anions, the more basic the oxide. Therefore, the oxygen partial negative charge reflects the electron donor properties of the oxygen in a single component oxide. Lopez et al. [50] suggested that Cu bonds ionically to MgO and forms a stable Cu–O–Mg species. These authors claimed that Cu gains a large net positive charge while the Cu electron is transferred to MgO. This more likely leads to an increase in the oxygen partial negative charge in MgO and could explain the increase in the catalyst basic site density after Cu addition to MgO. The oxygen partial negative charge increased in the order $Cs_2O > K_2O >$ MgO according to calculations made by Diez et al. [40,42]. The basicity trend of the present study is in good agreement with these calculations.

Since the catalyst basicity is expected to play an important role in the formation of the first C–C bond in ethanol synthesis from syngas and methanol [14,24–28] a comparison of the basicity of the present catalysts to conventional Cu–ZnO-based catalysts is important. Cu–ZnO–Zr_2O (Cu wt% = 41.20) has a reported intrinsic basicity of 0.4 μmol CO_2 m^{-2} [36], whereas in the present study the Cu–MgO intrinsic basicity was 4.3 μmol CO_2 m^{-2}. The intrinsic basicity of the Cu–MgO catalyst of the present study is approximately 11 times higher than that of Cu–ZnO–Zr_2O [36]. Addition of K or Cs to the Cu–MgO increased the intrinsic basicity further, with a value of 9.3 μmol CO_2 m^{-2} obtained for the 0.5 wt% K–Cu–MgO catalyst. The corresponding value for a 0.5 wt% K promoted Cu–ZnO–Al_2O_3 catalyst, measured at 196 K, was reported as 2.7 μmol CO_2 m^{-2} [12].

3.2. Product distribution over MgO-based catalyst

Previous work suggested that the formation of higher alcohols over Cu–ZnO-based catalysts is favoured at low H_2/CO ratios (≤1) [12,23,51,52]. Furthermore, isotopic tracer studies and NMR studies of ethanol synthesis from syngas and methanol over Cu–ZnO-based catalysts, suggested that CO is the main source of carbon in ethanol formation [27], whereas others have suggested that methanol is the main source of carbon in ethanol formation [14]. Hence, in the present work, initial catalyst testing was done in a CH_3OH/CO feed in the absence of H_2. The catalysts were tested at 101 kPa, 498 K, with a feed composition of He/CO/CH_3OH = 0.20/0.66/0.14 (molar) and contact time (W/F) of 12.3×10^{-3} g min (cm^3(STP))$^{-1}$. A summary of the product distribution and net conversion of reactants is given in Table 6. As expected, the total conversion of reactants over MgO was very low, whereas addition of Cu and alkali oxide to MgO increased the total conversion significantly. Note that in most cases the net CO consumption was negative, implying that the amount of CO incorporated into the formation of different carbonaceous products was less than the amount of CO generated by CH_3OH decomposition. In these cases, CO was treated as a product and its selectivity was included in the product selectivity calculations. The data of Table 6 show that the CO selectivity (S_{CO}) at 498 K decreased in the order: Cu–MgO > 0.5 wt% K–Cu–MgO > 0.5 wt% Cs–Cu–MgO, whereas the reverse order was observed for methyl formate (S_{MF}), CO_2 (S_{CO_2}) and C_2 (S_{C_2}) selectivities. The catalyst intrinsic basicity (Table 5) increased in the order Cu–MgO < 0.5 wt% K–Cu–MgO < 0.5 wt% Cs–Cu–MgO. Thus it can be concluded that an increase in the density of basic sites increased S_{MF} and S_{C_2}. However, comparing the 0.5 wt% K–Cu–MgO and the 4.4 wt% K–Cu–MgO as well as the 0.5 wt% Cs–Cu–MgO and the 13.5 wt% Cs–Cu–MgO catalysts, shows that increased K or Cs loading increased the S_{CO} and decreased in S_{MF} and S_{C_2}. Intrinsic basicity, however, increased with increased alkali metal loading (Table 5). Hence, among these catalysts, increased basic site density decreased S_{MF} and S_{C_2} and increased S_{CO}. Together, these data suggest that an optimum intrinsic basicity exists that maximizes selectivity to methyl formate and C_2 product species, as shown in Fig. 6. Note that changes in the catalyst intrinsic basicity were unavoidably accompanied by changes in Cu dispersion, S_{BET}, V_p and their impact on S_{MF}, S_{C_2} and S_{CO} is reflected in the scatter of the data of Fig. 6.

Table 5
Basic properties of MgO-based catalyst measured by means of CO_2 TPD.

Catalyst	Specific basicity (μmol CO_2 g^{-1})	Intrinsic basicity (μmol CO_2 m^{-2})	Distribution of different basic sites on the catalyst (%)		
			Weak	Medium	Strong
MgO	432.0	2.7	8	15	77
Cu–MgO	315.5	4.3	9	19	72
0.5 wt% K–Cu–MgO	392.4	9.3	11	21	69
0.5 wt% Cs–Cu–MgO	415.9	9.5	16	19	65
4.4 wt% K–Cu–MgO	403.0	13.4	16	13	71
13.5 wt% Cs–Cu–MgO	305.7	17.0	18	33	49

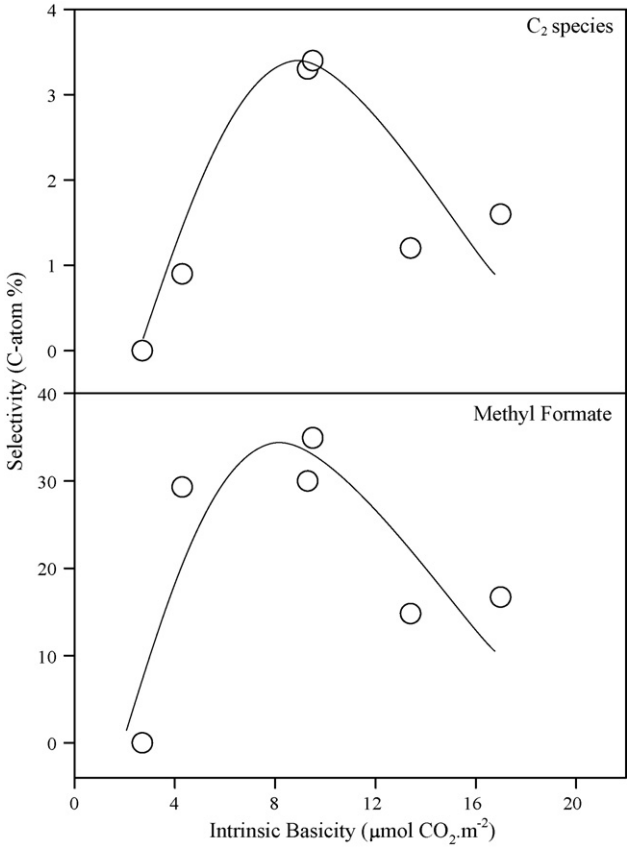

Fig. 6. Selectivity from reaction of CH_3OH/CO over alkali-promoted Cu–MgO catalysts as a function of their intrinsic basicity. Reaction conditions: 101 kPa, 498 K, feed composition He/CO/CH_3OH = 0.20/0.66/0.14 (molar) $W/F = 12.3 \times 10^{-3}$ min g $(cm^3(STP))^{-1}$, catalyst weight = 0.98 g.

The product distribution over the 0.5 wt% K–Cu–MgO and the 0.5 wt% Cs–Cu–MgO catalysts at 498 K and 523 K (Table 6), show that increased temperature increased S_{CO} whereas S_{MF} and S_{C_2} decreased, implying that lower operating temperature favoured C_2 species formation.

Since the 0.5 wt% Cs–Cu–MgO catalyst showed the highest selectivity towards C_2 species among all the tested catalysts, further experiments were conducted as a function of contact time (W/F) using this catalyst and the results are presented in Fig. 7. Also, to study the effect of Cs loading on the performance of the Cs promoted Cu–MgO catalyst, the same series of contact time experiments was performed on the 13.5 wt% Cs–Cu–MgO, and the results are shown in Fig. 8. For both the 0.5 wt% Cs–Cu–MgO and the 13.5 wt% Cs–Cu–MgO catalysts, it was observed that decreased contact time led to increased S_{MF} and decreased S_{CO}, whereas the S_{C_2} and S_{CO_2} remained almost unchanged. These observations imply that methyl formate was a primary product over both catalysts whereas CO was a secondary product, in agreement with previous studies [53,54].

The effect of different feed mixtures on the product distribution over the 13.5 wt% Cs–Cu–MgO catalyst was also examined using a feed of Ar/He/CH_3OH, CO/He/CH_3OH and H_2/He/CH_3OH and the results are shown in Table 7. The presence of either H_2 or CO in the feed stream compared to Ar, decreased the total conversion and the decrease in total conversion was more significant in the presence of H_2 than CO. Furthermore, the presence of H_2 in the feed decreased S_{MF} marginally, whereas the presence of CO in the feed, increased the S_{MF} compared to the presence of Ar in the feed. S_{C_2} decreased in the following order: H_2/He/CH_3OH > CO/He/CH_3OH > Ar/He/CH_3OH revealing that the presence of H_2, as opposed to CO and Ar in the feed, improved S_{C_2}, but note that the CH_3OH conversion decreased significantly in the H_2 rich atmosphere.

4. Discussion

The present study has demonstrated the preparation of high surface area MgO by thermal decomposition of $Mg(NO_3)_2$ in the presence of palmitic acid, and this method has been extended to alkali-promoted Cu–MgO catalysts. Using CO_2 TPD to quantify basicity, the alkali-promoted Cu–MgO was shown to have a higher intrinsic basicity than conventional Cu–ZnO catalysts and alkali-promoted Cu–ZnO catalysts. The surface area of the MgO (160 $m^2\ g^{-1}$) was significantly higher than the Cu–MgO (74 $m^2\ g^{-1}$), due mostly to pore blocking by the Cu. Further losses in surface area upon alkali promotion were shown to be due to both pore blocking and sintering effects. The latter was due to the higher calcination temperatures of the alkali promoted catalysts compared to the Cu–MgO.

Several reaction mechanisms have been proposed for the conversion of syngas to CH_3OH and other oxygenated products as well as for the conversion of CH_3OH to methyl formate, C_2 species (mainly ethanol), CO and CO_2. A summary of the most consistent mechanisms proposed in the literature regarding the formation of these products over Cu/metal oxide catalysts is shown in Figs. 9–11. In order to simplify these figures, the reaction pathways and intermediates containing carbon atoms are shown, whereas H, OH, H_2O and H_2 species are omitted. Results from the present study are conveniently discussed in view of some of these mechanistic proposals.

The present work showed that at 498 K on the high surface are MgO (Table 6) only, a small amount of the feed CH_3OH was con-

Table 6
Product distribution and catalyst activity over MgO-based catalysts using CO/He/CH_3OH feed.

Catalyst	Reaction temperature (K)	Net CO consumption (C-atom %)	Net CH_3OH conversion (C-atom %)	Total net conversion[a] (C-atom %)	Product selectivity (C-atom %)			
					CO	MF[b]	CO_2	C_2[c]
MgO	498	−1.2	6.4	5.3	100.0	0.0	0.0	0.0
Cu–MgO	498	−9.7	84.7	75.0	68.4	29.3	1.5	0.9
0.5 wt% K–Cu–MgO	498	−7.9	70.0	62.0	63.9	30.0	2.7	3.3
	523	−10.8	81.8	71.0	78.2	16.9	2.9	2.1
0.5 wt% Cs–Cu–MgO	498	−6.1	66.7	60.6	53.4	34.9	8.4	3.4
	523	−12.5	87.0	74.5	84.3	10.3	2.9	2.5
4.4 wt% K–Cu–MgO	498	−10.0	70.1	60.2	82.9	14.8	1.1	1.2
13.5 wt% Cs–Cu–MgO	498	−6.3	47.2	40.8	79.8	16.7	1.9	1.6

Reaction condition: 101 kPa, feed He/CO/CH_3OH = 0.20/0.66/0.14 molar, contact time (W/F) = 12.3×10^{-3} min g $(cm^3(STP))^{-1}$, catalyst weight = 0.98 g, v_0 = 84.4 $cm^3(STP)\ min^{-1}$.

[a] Total conversion = Net CO consumption + Net CH_3OH conversion.

[b] MF stands for methyl formate.

[c] C_2 stands for ethanol and acetic acid.

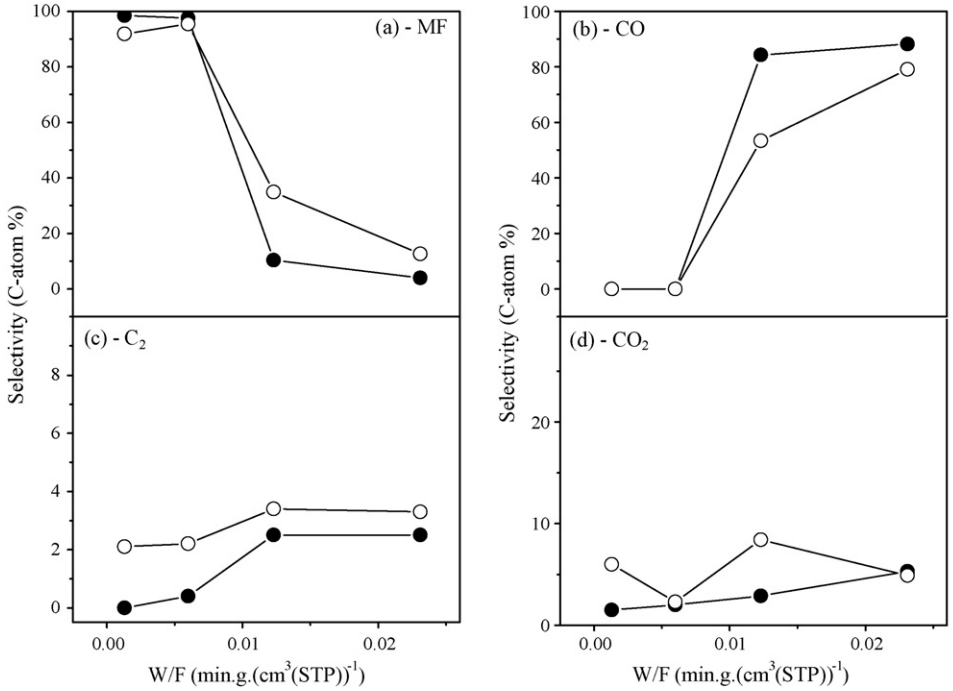

Fig. 7. Selectivity from reaction of CH_3OH/CO over 0.5 wt% Cs–Cu–MgO at (○) 498 K and (●) 523 K as a function of contact time (W/F) for: (a) methyl formate, (b) CO, (c) acetic acid and ethanol, (d) CO_2. Reaction conditions: 101 kPa, feed composition He/CO/CH_3OH = 0.20/0.66/0.14 (molar), v_0 = 84.4 cm^3(STP) min^{-1}.

verted to CO but no methyl formate, dimethyl ether (DME), other C_2 oxygenates or CO_2 was produced. Addition of Cu to the MgO resulted in a significant increase in conversion (from 5.3 to 75.0%, Table 6), with a high selectivity to methyl formate (29.3%) and CO (68.4%), and a low CO_2 (1.5%) and C_2 (0.9%) selectivity. Addition of the alkali promoters resulted in changes in the product selectivity, but in all cases, CO and methyl formate remained the major products. Clearly, although the basic MgO is able to convert CH_3OH to CO, most likely through the methoxy species shown in Path A-1 of Fig. 9, Cu is needed to obtain products other than CO. However, there is a well established synergy between the Cu and the metal oxide present in the catalyst [37] that influences product selectivity. In the present work, the basic MgO and alkali promoters ensure that no dimethyl ether is formed [30,37], and the selectivities to methyl formate, CO_2 and C_2 oxygenates were all dependent on the catalyst formulation (Table 6). Furthermore, both the reaction temperature

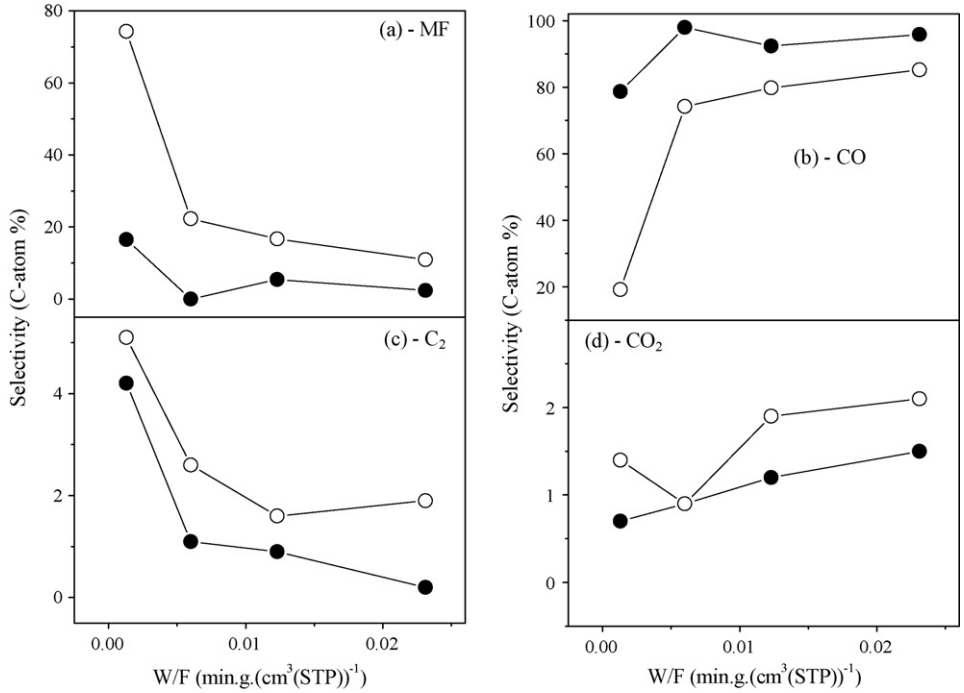

Fig. 8. Selectivity from reaction of CH_3OH/CO over 13.5 wt% Cs–Cu–MgO at (○) 498 K and (●) 523 K as a function of contact time (W/F) for: (a) methyl formate, (b) CO, (c) acetic acid and ethanol, (d) CO_2. Reaction conditions: 101 kPa, feed composition He/CO/CH_3OH = 0.20/0.66/0.14 (molar), v_0 = 84.4 cm^3(STP) min^{-1}.

Table 7
Product distribution and catalyst activity over 13.5 wt% Cs–Cu–MgO in different feed compositions.

Reaction temperature (K)	Feed mixture	Net CO consumption (C-atom %)	Net CH_3OH conversion (C-atom %)	Total conversion[a] (C-atom %)	Product selectivity (C-atom %)			
					CO	MF[b]	CO_2	C_2[c]
498	Ar/He/CH_3OH	0.0	48.2	48.2	81.7	15.2	2.9	0.2
	CO/He/CH_3OH	−6.3	47.2	40.8	79.8	16.7	1.9	1.6
	H_2/He/CH_3OH	0.0	6.6	6.6	79.5	13.6	3.3	3.6
523	Ar/He/CH_3OH	0.0	62.1	62.1	97.6	1.6	0.8	0.0
	CO/He/CH_3OH	−7.3	47.0	39.7	92.4	5.4	1.2	0.9
	H_2/He/CH_3OH	0.0	22.8	22.8	96.1	1.6	1.1	1.2

Reaction condition: 101 kPa, feed X/He/CH_3OH = 0.20/0.66/0.14 molar, where X is Ar or CO or H_2), contact time (W/F) = 12.3×10^{-3} min g $(cm^3(STP))^{-1}$, catalyst weight = 0.98 g, v_0 = 84.4 cm^3(STP) min^{-1}.
[a] Total conversion = Net CO consumption + Net CH_3OH conversion.
[b] MF stands for methyl formate.
[c] C_2 stands for ethanol and acetic acid.

and space velocity had a significant effect on the product selectivity. The data of Table 6 show that increased temperature resulted in higher methanol conversion and CO selectivity, with reduced selectivity to methyl formate and other C_2 oxygenates. Figs. 7 and 8 suggest that the initial product of reaction over the Cs–Cu–MgO catalyst was methyl formate, while CO was a secondary product. The selectivity to CO_2 was not a strong function of operating conditions.

Studies using ^{13}CO and $^{13}CO_2$ and H_2 as reactant have shown that CH_3OH is produced mainly from CO_2 and H_2 rather than CO and H_2 on Cu catalysts [10]. Hence, the methanol synthesis on Cu-based catalysts can be described by the following two parallel reactions [26,29]:

$$CO_2 + H_2 \leftrightarrow CO + H_2O \quad (1)$$

$$CO_2 + 3H_2 \leftrightarrow CH_3OH + H_2O \quad (2)$$

Most of the mechanistic studies on Cu catalysts agree that a formate species is formed from H_2 and CO_2 and further surface reaction leads to products CH_3OH and H_2O (the reverse of Path A-2 of Fig. 9) or CO and H_2O (Path B of Fig. 9) [24,26,29]. Carbon isotopic tracer studies have shown that the rate of the reverse water gas shift (Reaction (1)) is higher than the rate of CH_3OH synthesis from CO_2/H_2 (Reaction (2)) [29]. In the present work, no H_2O was added in the feed and consequently the reverse of Reaction (2) could not occur to any great extent. However, the data of Figs. 7 and 8 show that even at high space velocities some C_2 oxygenates were produced, and water is a co-product of these reactions. Consequently, the reverse of both Reactions (1) and (2) occur but to a limited extent because of the low levels of water generated as a consequence of C_2 formation. In the presence of water it is likely that a portion of the CH_3OH present in the feed decomposed to CO_2 via Path A-2 of Fig. 9. Alternatively, the forward or reverse reaction shown as Path B of Fig. 9 could occur, although this seems less likely in the present work given that the amount of CO_2 was not strongly dependent on the CO present in the feed (Table 7), nor on the C_2 selectivity (Figs. 7 and 8).

CH_3OH conversion to methyl formate over Cu-based catalysts has been well studied and it is known that Cu plays a significant role as active catalyst for methyl formate formation [29,30,54]. Fig. 10 shows potential routes to methyl formate, but the mechanisms that have received the most acceptance are the CH_3OH dimerization paths shown as Path C and D. Recent evidence based on H/D exchange experiments [55] and experiments using ^{13}C labelled methanol [56] suggested that methyl formate is generated via the nucleophilic attack of a surface methoxy species on a surface formyl species (Path C of Fig. 10) or a formate species (Path D of Fig. 10) [30,53–56]. Nunan et al. [14] provided thermodynamic and other arguments to suggest that methyl formate was generated by methanol carbonylation over their Cs–Cu–ZnO catalyst operated at high pressure (7.6 MPa). At the low pressure conditions of the present study, however, the methyl formate generated was about three orders of magnitude greater than the equilibrium yield from methanol carbonylation ($CH_3OH + CO \rightarrow HCOOCH_3$ $K_{Eq}^{598\,K} = 2.11 \times 10^{-4}$ versus $K_{Calc}^{598\,K} = 3.45 \times 10^{-1}$), whereas it was less than the methanol dimerization equilibrium yield ($2CH_3OH \rightarrow HCOOCH_3 + 2H_2$ $K_{Eq}^{598\,K} = 3.14 \times 10^{-2}$ versus $K_{Calc}^{598\,K} = 2.22 \times 10^{-2}$). The methanol dimerization reaction to methyl formate and hydrogen could occur directly from methoxy and formyl species derived from CH_3OH interacting with Cu as well as the basic sites of the present catalysts. Other studies on the effect of the state of Cu on methyl formate formation have suggested that CH_3OH decomposes to CO via a methyl formate intermediate over Cu^0, but no clear mechanism was proposed for this step [53,54]. In the present work it is likely that surface formyl, methoxy and formate all exist on the catalyst surface. Path C and Path D of Fig. 10 yield methyl formate as a primary product. Subsequent decomposition of methyl formate to CH_3OH and CO, or to CO and H_2, would yield CO as a secondary product, in agreement with the experimental observations of Figs. 7 and 8. Hence it is likely that in the present study, part of the CH_3OH present in the feed stream was decomposed to CO via methyl formate over Cu^0.

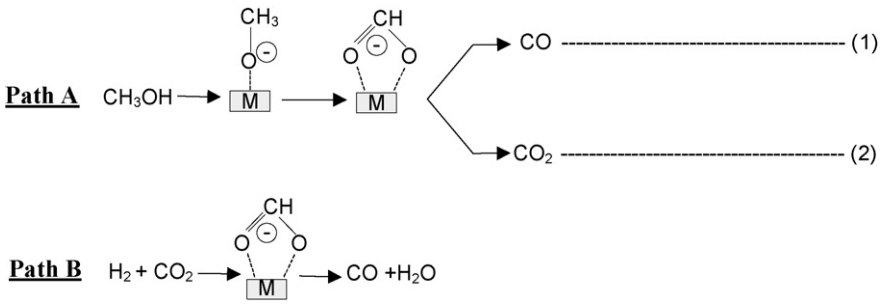

Fig. 9. Pathway for: (A-1) CH_3OH decomposition to CO, (A-2) CH_3OH decomposition to CO_2 [24,26,29], (B) reverse water gas shift [29]. M stands for Cu^0 or metal cation.

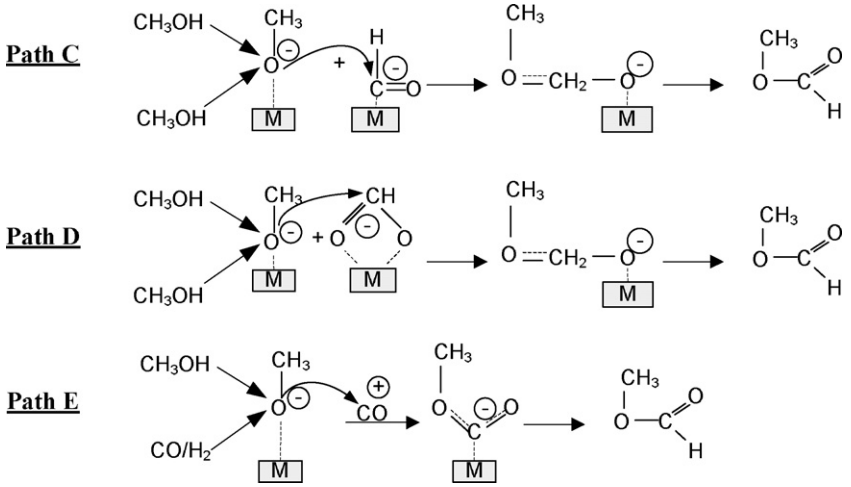

Fig. 10. Pathway for: (C) CH_3OH dimerization to methyl formate via methoxy and formyl intermediates [55,56], (D) CH_3OH dimerization to methyl formate via methoxy and formate intermediates [55,56], (E) CH_3OH carbonylation to methyl formate [14]. M stands for Cu^0 or metal cation.

Results of the present work showed that an increase in catalyst intrinsic basicity up to 9.5 μmol CO_2 m^{-2} at low Cu dispersion (<1.54%), led to an increase in S_{MF} (Fig. 6). The methyl formate selectivity decreased in the order: 0.5 wt% Cs–Cu–MgO > 0.5 wt% K–Cu–MgO ≈ Cu–MgO. Also, addition of CO to CH_3OH in the feed led to a small increase in S_{MF}. The formation of methyl formate via nucleophilic attack by methoxide species on formyl species would be enhanced by increased basicity of the catalyst, as has been observed. An increase in catalyst intrinsic basicity also led to a small increase in S_{C_2}. Xu and Iglesia [27] have suggested that nucleophilic attack of the methyl formate by surface CH_3OCO^- species on a basic catalyst (metal cation) leads to the formation of an initial C–C bond that yields ethanol following several hydrogenation steps that are not shown in Path F-1 of Fig. 11. Other mechanistic studies suggest that the nucleophilic attack of an adsorbed formyl species with formaldehyde on a basic site leads to the formation of the initial C–C bond which subsequently yields ethanol (Path G of Fig. 11) [14]. Noting that formaldehyde was absent in both the feed and product streams of the present study, it is likely an increase in the catalyst intrinsic basicity led to a nucleophilic attack of the methyl formate by surface CH_3OCO^- species on a basic site, leading to ethanol formation and a small increase in C_2 formation (S_{C_2} < 5 C-atom %). Results of the present work showed that S_{C_2} decreased in the order: 0.5 wt% Cs–Cu–MgO ≈ 0.5 wt% K–Cu–MgO > Cu–MgO suggesting that Path F-1 of Fig. 11 took place over Cu/Mg^{2+} and addition of Cs_2O and K_2O to Cu–MgO provided stronger basic sites (Cs^+ and K^+) for this reaction pathway.

To the authors knowledge, only one previous study has reported the formation of acetic acid from CH_3OH/CO over Cu-based catalysts [14]. The only mechanistic studies available for acetic acid synthesis suggest that nucleophilic attack of CO on methoxide over a basic site leads to CH_3OCO^- species. The rearrangement of CH_3OCO^- species to acetate species (CH_3COO^-) leads to C–C bond formation, and a final hydrogenation step yields acetic acid (Path F-2 of Fig. 11) [14]. However, Nunan et al. [14] noted that the rearrangement step ($CH_3OCO^- \rightarrow CH_3COO^-$) had high activation energy (based on an analysis of gas phase reactions) and was not very likely to occur. In the present study, the increase in the catalyst intrinsic basicity up to 7.5 μmol CO_2 m^{-2} led to a small

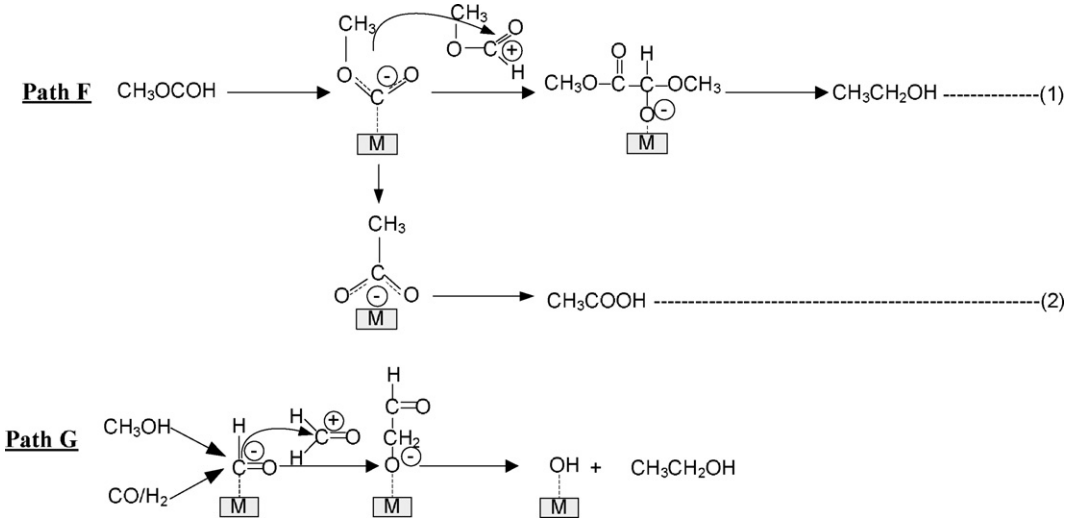

Fig. 11. Pathway for: (F-1) ethanol formation from methyl formate [27], (F-2) acetic acid formation from methyl formate [14], (G) ethanol formation from CH_3OH and CO [14]. M stands for Cu^0 or metal cation.

increase in the S_{C_2} and it is likely that the high intrinsic basicity of the alkali-promoted Cu–MgO catalysts facilitated the formation of small amounts of acetic acid (acetic acid selectivity < 3 C-atom %) on the catalyst surface as shown by Path F-2 of Fig. 11.

The correlation between intrinsic basicity and S_{MF}, S_{C_2} and S_{CO} identified in the present study (Fig. 6), suggests that at low Cu dispersion (<1.54%), an increase in the intrinsic basicity up to 9.5 μmol CO_2 m^{-2}, leads to an increase in S_{MF} and S_{C_2}, while a further increase in the intrinsic basicity leads to a decrease in S_{MF} and S_{C_2}. (In both cases the opposite trend was observed for S_{CO} compared to S_{MF} and S_{C_2}.) As discussed earlier, methyl formate and C_2 species were most likely formed from methoxy, formyl and formate species adsorbed on the Cu/metal oxide and that nucleophilic attack lead to methyl formate and C_2 oxygenates. Subsequently, methyl formate was likely converted to CH_3OH and CO on Cu^0. Based on these observations and the correlation between intrinsic basicity and S_{MF}, S_{C_2} and S_{CO}, it can be speculated that a balance of metal and basic sites are required for maximum selectivity to methyl formate and C_2 oxygenates. At very high intrinsic basicities (the high loading K or Cs promoted Cu–MgO with intrinsic basicity > 9.5 μmol CO_2 m^{-2}), although the formation of the methoxy species may be enhanced, the formyl and formate species would be reduced because of a reduced Cu surface area (Table 3). Note that Nunan et al. [14] also studied the effect of Cs loading on Cs–Cu–ZnO catalysts for methyl formate formation from syngas and concluded that there was an optimum Cs loading at which methyl formate yield reached a maximum value, in agreement with the present observations made regarding the effect of Cs loading on the Cs–Cu–MgO catalyst.

Hsiao and Lin [37] have studied the synthesis of methyl formate and higher alcohols over Cu–MgO–Al_2O_3 (Cu/MgO/Al_2O_3 = 4/5/91 wt%) at 523 K, 101 kPa and $W/F = 106.1 \times 10^{-3}$ min g $(cm^3(STP))^{-1}$). The study reported a total conversion of 82% with CO, CO_2 and CH_3OCH_3 as the only products. The catalyst showed no activity towards methyl formate or C_2 species, whereas over Cu–MgO in the present study, high selectivity towards methyl formate (S_{MF} = 29.3%, Table 6) and low selectivity towards C_2 species (S_{C_2} = 0.9%, Table 6) was observed. The low Cu (4 wt%) and MgO (5 wt%) content of the Cu–MgO–Al_2O_3 catalyst used by Hsiao and Lin [37] and the presence of the acidic Al_2O_3 support, results in the formation of CH_3OCH_3, generated by the acid catalysed dehydration of methanol. The S_{BET} and Cu dispersion for Cu–MgO–Al_2O_3 were reported as 115 m^2 g^{-1} and 60%, respectively [37], whereas for the Cu–MgO of the present work, values of 74 m^2 g^{-1} and 1.54%, respectively were obtained (Tables 2 and 3). These distinct differences, together with the higher temperature and W/F used by Hsiao and Lin [37] account for the differences in product distributions between the two studies.

5. Conclusion

High surface area MgO, Cu–MgO and alkali (K_2O and Cs_2O) promoted Cu–MgO were prepared by thermal decomposition of metal salts in the presence of palmitic acid. The basicity of the catalysts decreased in the order: 13.5 wt% Cs–Cu–MgO > 4.4 wt% K–Cu–MgO > 0.5 wt% Cs–Cu–MgO > 0.5 wt% K–Cu–MgO > Cu–MgO > MgO. The intrinsic basicity of the Cu–MgO and alkali-promoted Cu–MgO catalysts were more than 10 times greater than a conventional Cu–ZnO catalyst. Over the alkali-promoted Cu–MgO catalysts at 101 kPa and 498 K with a CO/He/CH_3OH (0.20/0.66/0.14) feed gas, methyl formate was the primary product while CO was a secondary product. C_2 species were also produced with low selectivity (S_{C_2} < 5%). Formation of methyl formate and C_2 species were attributed to basic sites and Cu^0 and there was an optimum basicity (9.5 μmol CO_2 m^{-2}) at which the S_{MF} and S_{C_2} reached a maximum.

Acknowledgements

Financial support from Natural Sciences and Engineering Research Council (NSERC) of Canada is gratefully acknowledged.

References

[1] J.R. Rostrup-Nielsen, Science 308 (2005) 1421.
[2] V. Subramani, S.K. Gangwal, Energy Fuels 22 (2008) 814.
[3] K. Klier, V. Chatikavanij, R.G. Herman, G.W. Simmons, J. Catal. 74 (1982) 343.
[4] K. Klier, Adv. Catal. 30 (1982) 243.
[5] J.C.J. Bart, R.P.A. Sneeden, Catal. Today 2 (1987) 1.
[6] G.W. Bridger, M.S. Spencer, in: M.V. Twigg (Ed.), Catalyst Hand Book, 2nd ed., Wolfe Publ. Co., London, England, 1989, p. 441.
[7] R.G. Herman, in: L. Guczi (Ed.), New Trends in CO Activation, Elsevier, Amsterdam, 1991, p. 265.
[8] J.R. LeBlanc, R.V. Schneider III, R.B. Strait, in: W.-H. Cheng, H.H. Kung (Eds.), Methanol Production and Use, Marcel Dekker, New York, 1994, p. 51.
[9] P.B. Rasmussen, P.M. Holmbald, T. Askgaard, C.V. Ovesen, P. Stoltze, J.K. Norskov, I. Chorkendorff, Catal. Lett. 26 (1994) 373.
[10] G.C. Chinchen, P.J. Denny, J.R. Jennings, M.S. Spencer, K.C. Waugh, Appl. Catal. 36 (1987) 1.
[11] K.J. Smith, R.B. Anderson, J. Catal. 85 (1984) 428.
[12] K.J. Smith, R.B. Anderson, Can. J. Chem. Eng. 61 (1983) 40.
[13] E. Tronconi, N. Ferlazzo, P. Forzatti, I. Pasquon, Ind. Eng. Chem. Res. 26 (1987) 2122.
[14] J.G. Nunan, C.E. Bogdan, K. Klier, K.J. Smith, C.W. Young, R.G. Herman, J. Catal. 113 (1988) 410.
[15] D.J. Elliot, F.J. Pennella, J. Catal. 114 (1988) 90.
[16] K.J. Smith, C.W. Young, R.G. Herman, K. Klier, Ind. Eng. Chem. Res. 30 (1991) 61.
[17] R.G. Herman, Catal. Today 55 (2000) 233.
[18] H. Trevino, Guan-Dao Lei, W.M.H. Sachtler, J. Appl. Catal. 154 (1995) 245.
[19] C.R. Apesteguia, B.D. Rites, S. Miseo, S. Soled, Catal. Lett. 44 (1997) 1.
[20] J.G. Nunan, C.E. Bogdan, R.G. Herman, K. Klier, Catal. Lett. 2 (1989) 49.
[21] R. Xu, C. Yang, W. Wei, Wen-huai Li, Yu-han Sun, Tian-dou Hu, J. Mol. Catal. A: Chem. 221 (2004) 51.
[22] J.G. Nunan, C.E. Bogdan, K. Klier, K.J. Smith, Chyi-Woei Young, R.G. Herman, J. Catal. 116 (1989) 195.
[23] G.A. Vedage, P.B. Himelfarb, G.W. Simmons, K. Klier, Am. Chem. Soc. Symp. Ser. 279 (1985) 295.
[24] T.S. Askgaard, J.K. Norskov, C.V. Ovesen, P. Stoltze, J. Catal. 156 (1995) 229.
[25] D.B. Clarke, A.T. Bell, J. Catal. 154 (1995) 314.
[26] S. Fujita, M. Usui, H. Ito, N. Takezawa, J. Catal. 157 (1995) 403.
[27] M. Xu, E. Iglesia, Catal. Lett. 51 (1988) 47.
[28] M. Xu, E. Iglesia, J. Catal. 188 (1999) 125.
[29] Y. Yang, C.A. Mims, R.S. Disselkamp, D. Mei, Ja-Hun Kwak, J. Szanyi, C.H.F. Peden, C.T. Campbell, Catal. Lett. 125 (3–4) (2008) 201.
[30] S. Sato, M. Iijima, T. Nakayama, T. Sodesawa, F. Nozaki, J. Catal. 169 (1997) 447.
[31] J. Nunan, K. Klier, C.W. Young, P.B. Himelfarb, R.G. Herman, J. Chem. Soc., Chem. Commun, (1986) 193.
[32] V.K. Diez, C.R. Apesteguia, J.I. Di Cosimo, Catal. Today 63–1 (2000) 53.
[33] M. Bolognini, F. Cavani, D. Scagliarini, C. Flego, C. Perego, M. Saba, Catal. Today 75 (2002) 103.
[34] J.I. Di Cosimo, V.K. Diez, C.R. Apesteguia, Appl. Catal. A 137 (1996) 149.
[35] M. Di Serio, M. Ledda, M. Cozzolino, G. Minutillo, R. Tesser, E. Santacesaria, Ind. Eng. Chem. Res. 45 (2006) 3009.
[36] F. Arena, G. Italiano, K. Barbera, S. Bordiga, G. Bonura, L. Spadaro, F. Frusteri, Appl. Catal. A 350 (2008) 16.
[37] T.C. Hsiao, S.D. Lin, Catal. Lett. 119 (2007) 72.
[38] S. Takenaka, R. Takahashi, T. Sodesawa, Phys. Chem. Chem. Phys. 5 (2003) 4968.
[39] H. Hattori, Appl. Catal. A 222 (2001) 247.
[40] V.K. Diez, C.R. Apesteguia, J.I. Di Cosimo, Catal. Today 63 (2000) 53.
[41] C. Chizallet, G. Costenin, M. Che, F. Delbecq, P. Sautet, J. Am. Chem. Soc. 129 (2007) 6442.
[42] V.K. Diez, C.R. Apesteguia, J.I. Di Cosimo, J. Catal. 240 (2006) 235.
[43] CRC Handbook of Chemistry and Physics, 89th Edition, 2008–2009, pp. 4-57 & 4-83.
[44] B.M. Nagaraja, A.H. Padmasri, B. David Raju, K.S. Rama Rao, J. Mol. Catal. A: Chem. 265 (2007) 90.
[45] Hua-Hsien Liao, Li-Min Chen, Z. Xu, G. Li, Y. Yang, Appl. Phys. Lett. 92 (173303) (2008) 1.
[46] F. Chang, W. Kuo, K. Lee, Appl. Catal. A 246 (2003) 253.
[47] B.M. Nagaraja, V.S. Kumar, V. Shashikala, A.H. Padmasri, S.S. Reddy, B.D. Raju, K.S.R. Rao, J. Mol. Catal. A: Chem. 223 (2004) 339.
[48] M. Varga, A. Molnar, G. Mulas, M. Mohai, I. Bertoti, G. Cocco, J. Catal. 206 (2002) 71.
[49] A.S. Ahmed, Egypt. J. Chem. 50 (2) (2007) 223.

[50] N. Lopez, F. Illas, J. Phys. Chem. 100 (1996) 16275.
[51] K. Klier, R.G. Herman, C.W. Young, Div. Fuel Chem. ACS 29 (5) (1984) 273 (Preprint).
[52] G. Natta, U. Colombo, I. Pasquon, in: P.H. Emmett (Ed.), Catalysis, vol. 5, Reinhold, New York, 1957, p. 131.
[53] A.Ya. Rozovskii, Kinet. Catal. 44 (3) (2003) 360.
[54] T. Tsoncheva, Tz. Venkov, M. Dimitrov, C. Minchev, K. Hadjiivanov, J. Mol. Catal. A: Chem. 209 (2004) 125.
[55] L. Domokos, T. Katona, A. Molnar, Catal. Lett. 40 (1996) 215.
[56] M.-J. Chung, D.-J. Moon, K.-Y. Park, S.-K. Ihm, J. Catal. 136 (1992) 609.